The comparative importance of *DE*3, *SE*2, and *SPW*4 on the generation of wavenumber-4 longitude structures in the low-latitude ionosphere during September equinox

N. M. Pedatella,[1] M. E. Hagan,[1] and A. Maute[1]

Received 22 August 2012; revised 12 September 2012; accepted 12 September 2012; published 13 October 2012.

[1] Numerical simulations are performed to investigate the generation of the wave-4 longitude variation in the low-latitude ionosphere due to the diurnal eastward propagating nonmigrating tide with zonal wavenumber 3 (*DE*3), semidiurnal eastward propagating nonmigrating tide with zonal wavenumber 2 (*SE*2), and stationary planetary wave 4 (*SPW*4). From a fixed local time perspective, the *DE*3, *SE*2, and *SPW*4 all appear as wave-4 structures in longitude, and thus each of these waves must be considered as a potential source of the wave-4 variation in the ionosphere. Both the *DE*3 and *SPW*4 are found to produce significant wave-4 variations in the equatorial vertical $\mathbf{E} \times \mathbf{B}$ drift velocity, and in the ionospheric peak density (NmF2) at 15°N magnetic latitude. The daytime wave-4 variation in NmF2 is driven by the combination of vertical $\mathbf{E} \times \mathbf{B}$ drift variability and in-situ effects due largely to meridional neutral winds. The simulation results indicate that the *SE*2 is not a contributor to the wave-4 longitude variation. Our results further demonstrate that the actual wave-4 longitude variation is due to a combination of the *DE*3 and *SPW*4. We therefore conclude that, in addition to the *DE*3, the *SPW*4 also needs to be considered as an important driver of the wave-4 longitude variation in the low-latitude ionosphere. We additionally present evidence for the generation of the *SPW*4 due to the nonlinear interaction between the migrating diurnal tide and the *DE*3, and demonstrate the impact of *DE*3 variability on the amplitude of the *SPW*4. **Citation:** Pedatella, N. M., M. E. Hagan, and A. Maute (2012), The comparative importance of *DE*3, *SE*2, and *SPW*4 on the generation of wavenumber-4 longitude structures in the low-latitude ionosphere during September equinox, *Geophys. Res. Lett.*, *39*, L19108, doi:10.1029/2012GL053643.

1. Introduction

[2] From a fixed local time perspective, the low-latitude ionosphere exhibits a notable wavenumber-4 (hereafter wave-4) variation in longitude near September and March equinoxes. The wave-4 structure has been observed in ionospheric airglow [e.g., *Immel et al.*, 2006], total electron content (TEC) [e.g., *Scherliess et al.*, 2008], and electron densities near the ionosphere peak height [e.g., *Lin et al.*, 2007]. *Immel et al.* [2006] first suggested that the wave-4 variation in the ionosphere was due to zonal wind modulation of E-region electric fields by the diurnal eastward propagating nonmigrating tide with zonal wavenumber-3 (*DE*3). The *DE*3 is generated by the longitude dependence of latent heating due to deep convection in the tropics [*Hagan and Forbes*, 2002]. Both observations [*Forbes et al.*, 2008] and numerical model results [*Hagan et al.*, 2007] illustrate that the *DE*3 propagates vertically, and achieves large amplitudes in the ionospheric E-region where it may modulate the dynamo generation of electric fields. The hypothesis put forth by *Immel et al.* [2006] that the source of the wave-4 variation lies in modulation of E-region electric fields by the *DE*3 has thus been considered an extremely probable scenario. This connection has been further supported by the similar seasonal variation of the *DE*3 and wave-4 longitude structure [*Fang et al.*, 2009]. Additionally, observations reveal significant wave-4 longitude variations in the equatorial electrojet and vertical $\mathbf{E} \times \mathbf{B}$ drift velocities [*England et al.*, 2006; *Fejer et al.*, 2008], demonstrating that modulation of E-region electric fields is a likely source for the wave-4 variations in the F-region ionosphere. The *DE*3, and other waves, can also propagate directly into the thermosphere [e.g., *Oberheide et al.*, 2011], leading to an ionospheric wave-4 longitude variation that is driven in-situ by changes in neutral composition and/or meridional neutral winds [*England et al.*, 2010]. In the F-region ionosphere, the wave-4 longitude variation may thus be driven by a combination of changes in vertical $\mathbf{E} \times \mathbf{B}$ drifts, neutral composition, and neutral winds.

[3] The aforementioned studies have predominantly focused on the *DE*3 as the source of the wave-4 variation in the ionosphere. However, when observed from a fixed local time perspective, a number of other waves can also produce a wave-4 longitude variation, and it is important to consider the possibility that these waves may play a role in generating wave-4 longitude variability in the ionosphere. In particular, numerical models and observations reveal that both the semidiurnal eastward propagating nonmigrating tide with zonal wavenumber 2 (*SE*2) and stationary planetary wave 4 (*SPW*4) achieve relatively large amplitudes at E-region altitudes [*Hagan et al.*, 2009; *Oberheide et al.*, 2011]. Therefore, in addition to the *DE*3, it is important to consider the potentially significant role that the *SE*2 and *SPW*4 may play in generating the ionospheric wave-4 longitude variation. The objective of the present study is to elucidate the contribution of the *DE*3, *SE*2, and *SPW*4 on generating the wave-4 longitude variability in the low-latitude ionosphere. We note that other tides also appear as a wave-4 longitude structure when observed from a fixed local time perspective. However, they are unlikely to contribute to the ionosphere

[1]High Altitude Observatory, National Center for Atmospheric Research, Boulder, Colorado, USA.

Corresponding author: N. M. Pedatella, High Altitude Observatory, National Center for Atmospheric Research, PO Box 3000, Boulder, CO 80307-3000, USA. (nickp@ucar.edu)

0094-8276/12/2012GL053643

Table 1. The Simulated Cases Along With the Combination of Tides and Stationary Planetary Waves That Are Used to Reconstruct the Thermosphere for Each Case[a]

Case	Tides and Stationary Planetary Waves Included in Simulation
Control	Migrating tides
Realistic	All tides and stationary planetary waves
*DE*3	Migrating tides plus *DE*3
*rDE*3	Migrating tides plus reduced *DE*3[b]
*DE*3*nodyn*	Migrating tides plus *DE*3[c]
*SPW*4	Migrating tides plus *SPW*4
*rSPW*4	Migrating tides plus reduced *SPW*4[b]
*SPW*4*nodyn*	Migrating tides plus *SPW*4[c]
*SE*2	Migrating tides plus *SE*2
*DE*3 + *SPW*4	Migrating tides plus *DE*3 and *SPW*4

[a]Note that the zonal mean is included in all cases.
[b]The amplitude is reduced by 50% throughout the model domain.
[c]Model is run using vertical $\mathbf{E} \times \mathbf{B}$ drift velocities from *Scherliess and Fejer* [1999].

wave-4 variation [e.g., *Oberheide et al.*, 2011]. In the present study we therefore limit our attention to the *DE*3, *SE*2, and *SPW*4. The impact of these waves on the longitudinal variability in the ionosphere is investigated through a series of numerical simulations using an ionosphere-electrodynamics model. Additionally, since the *SPW*4 is thought to be generated by the nonlinear interaction of *DE*3 and the migrating diurnal tide *DW*1, we perform simulations to investigate the impact of *DE*3 variability on the *SPW*4.

2. Numerical Models

2.1. NCAR TIME-GCM

[4] The National Center for Atmospheric Research (NCAR) Thermosphere-Ionosphere-Mesosphere-Electrodynamics General Circulation Model (TIME-GCM) is a three-dimensional first principles model of the mesosphere, thermosphere, and ionosphere with self-consistent electrodynamics. The TIME-GCM encompasses an altitude range of ~30 km to 400–700 km. The upper boundary height varies depending upon solar conditions due to the use of a pressure coordinate system in the vertical direction. Further details regarding the TIME-GCM can be found in *Roble* [1995] and *Roble and Ridley* [1994]. The simulations use a horizontal resolution of 2.5° in latitude and longitude, and a vertical resolution of 4 grid points per scale height. Similar to *Hagan et al.* [2009], we simulate solar minimum (F10.7 = 75) and September equinox conditions when the *DE*3 and *SPW*4 are known to obtain large amplitudes [e.g., *Oberheide et al.*, 2011].

[5] The TIME-GCM lower boundary is forced with diurnal and semidiurnal migrating and nonmigrating tides based on the Global Scale Wave Model (GSWM-02) [*Hagan and Forbes*, 2002, 2003]. Note that we have added six hours to the phase of the GSWM-02 *DE*3 at the model lower boundary so that the simulated *DE*3 phase is in agreement with observations near 100 km [e.g., *Forbes et al.*, 2008]. Shifting the phase may be necessary due to the neglect of radiative forcing of the *DE*3 in the GSWM-02, and the adjusted phase at the model lower boundary is in better agreement with the latest version of the GSWM which incorporates radiative heating [*Zhang et al.*, 2010]. Stationary waves are not specified at the model lower boundary, and thus the *SPW*4 must be generated due to processes internal to the model. The *SPW*4 in the TIME-GCM is thought to be generated by a nonlinear tide-tide interaction. The nonlinear interaction of two tides will produce two additional waves with zonal wavenumbers and frequencies that are sums and differences of the zonal wavenumbers and frequencies of the two interacting tides [*Teitelbaum and Vial*, 1991]. The nonlinear interaction between the *DW*1 and *DE*3 will thus produce the *SPW*4, and also the *SE*2. *Hagan et al.* [2009] attributed the *SPW*4 in the TIME-GCM to be due to this nonlinear interaction, while the *SE*2 may be due to both nonlinear interaction and tropospheric latent heat release. Since the *DE*3 and *DW*1 generate the *SPW*4, these waves cannot necessarily be considered as independent, and variations in the *DE*3 or *DW*1 may drive changes in the *SPW*4. To further understand the sensitivity of the *SPW*4 to variability in the *DE*3, an additional TIME-GCM simulation is performed where the amplitude of the *DE*3 forcing at the model lower boundary is reduced by 50%.

2.2. Ionosphere-Electrodynamics Model

[6] To assess the importance of different tides and stationary waves on generating the wave-4 longitude variation in the low-latitude ionosphere, we make use of a coupled ionosphere-electrodynamics model. The model consists of the Global Ionosphere Plasmasphere (GIP) model [*Millward et al.*, 2007] coupled to the electrodynamics portion of the NCAR Thermosphere-Ionosphere-Electrodynamics General Circulation Model (TIE-GCM). In the present study we use the TIME-GCM thermosphere (composition, temperature, and winds) to drive the ionosphere-electrodynamics model for the representative September day. This is done by first extracting the migrating and nonmigrating tides, and stationary waves from the TIME-GCM simulation results. The thermosphere is then reconstructed based on the zonal means and a subset of the tides and stationary waves, allowing us to isolate the effect that individual components have on generating longitude variability. We present results for several different simulations where the thermosphere is reconstructed using different combinations of tides and stationary waves. The specific cases considered are listed in Table 1. Note that throughout the following, we will refer to the individual cases by their names provided in Table 1. For the two reduced amplitude cases, we have decreased the amplitude by 50% throughout the model domain.

3. Results and Discussion

[7] Longitude variations of the daytime vertical $\mathbf{E} \times \mathbf{B}$ drift velocity at the magnetic equator and 300 km altitude are presented in Figure 1a. Note that the equatorial results presented herein should be considered as representative of the longitudinal variations that occur throughout the low-latitude ionosphere. In Figure 1a, the vertical $\mathbf{E} \times \mathbf{B}$ drift velocities are averaged between 12 and 15 local time. This local time corresponds to the maximum daytime vertical drifts in the model simulations. The results are presented for the ionosphere-electrodynamics model for all of the cases considered, as well as for the TIME-GCM simulation. The TIME-GCM results have been offset by 3 ms^{-1} so that the absolute $\mathbf{E} \times \mathbf{B}$ drifts are in closer agreement between the two models. The longitude variation simulated by the TIME-GCM (Figure 1a, solid grey) agrees well with the ionosphere-electrodynamics model results for the realistic

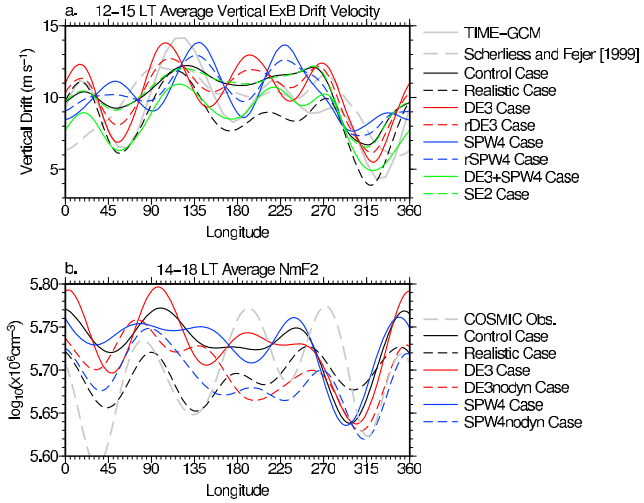

Figure 1. (a) Longitude variation of the simulated vertical **E** × **B** drift velocity at the magnetic equator and 300 km altitude. The results shown are for the average between 12 and 15 local time. Individual lines correspond to the TIME-GCM simulation results, climatology from *Scherliess and Fejer* [1999], and the simulation results for the ionosphere-electrodynamics model. Note that 3 ms^{-1} has been subtracted from the TIME-GCM results and the climatological values from *Scherliess and Fejer* [1999]. (b) Longitude variation of the ionospheric peak density (NmF2) at 15° magnetic latitude. The results are for the average between 14 and 18 local time. The individual lines correspond to simulation results for different cases that are specified in Table 1.

case (Figure 1a, dashed black). However, there are a few minor differences which may be due to differences in the ionosphere between these two models. Differences between the two models may also be responsible for the ∼3 ms^{-1} absolute difference in the daytime vertical **E** × **B** drift velocity. Nonetheless, the generally good agreement validates our approach, and demonstrates that the ionosphere-electrodynamics model can reliably reproduce the longitude variations in the low-latitude ionosphere despite the fact that our results are not based on a self-consistent ionosphere and thermosphere. The results for the realistic case and the TIME-GCM simulation reveal that the maximum vertical **E** × **B** drift velocities occur near 15°, 120°, 220°, and ∼270–290°. This is in good agreement with the observed longitude variation at equinox [e.g., *Fejer et al.*, 2008], further validating our simulations.

[8] The results in Figure 1a clearly illustrate the relative importance of migrating tides, *DE*3, *SE*2, and *SPW*4 on generating longitude variations in the daytime vertical **E** × **B** drift velocity. When observed from a fixed local time perspective migrating tides are longitudinally invariant; however, the simulation results for the control case (solid black) indicate that migrating tides alone produce considerable longitude variability. These longitude variations arise due to the effects of the geomagnetic field on ion-neutral coupling processes. The primary cause of the longitude variability is related to the offset between the geomagnetic and geographic poles. This results in the migrating tides, which are generally symmetric with respect to the geographic equator, having a wavenumber-1 structure in longitude when viewed relative to the geomagnetic equator. Additional variability may arise due to the geomagnetic field declination and main field strength. Results for the *SE*2 case (dashed green) are nearly identical to those from the control simulation, indicating that the *SE*2 does not contribute to the longitude variability. The absence of any *SE*2 contribution to the longitude variability may be attributed to its generally small amplitude (<10 ms^{-1}) combined with the fact that the *SE*2 peaks near 95–100 km, which is below the peak conductivities of the dynamo region. For the *DE*3 case (solid red), the simulations reveal clear peaks near 15°, 100°, 190°, and 270° longitude. However, there are considerable differences in the longitude variability due solely to the *DE*3 and the longitude variation that is simulated in the realistic case. This difference is most evident in the locations of the maxima and minima between ∼90–230° longitude. We therefore conclude that the *DE*3 is not the only contributor to the wave-4 variation. A notable wave-4 longitude variation is apparent in the simulation results for the *SPW*4 case. This demonstrates that the *SPW*4 is also capable of modulating the dynamo generation of electric fields in the E-region, and that the *SPW*4 may be a potentially important contributor to the wave-4 longitude variation. However, it is again apparent that the *SPW*4 alone does not fully reproduce the complete longitude variability. The simulation results for the *DE*3 + *SPW*4 case (solid green) yield a longitude variation that is fairly similar to the realistic case. We note that while the *DE*3 alone captures a majority of the wave-4 longitude variation, the addition of the *SPW*4 shifts the location of some of the maxima/minima in longitude, leading to an improved representation of the longitude variation. The addition of the *SPW*4 also results in a reduction of the longitude variability compared to the simulation results with only the *DE*3. The wave-4 longitude variability in the low-latitude ionosphere thus appears to be driven primarily by the combined effect of *DE*3 and *SPW*4. However, there remain some comparatively small differences in the longitude variability, suggesting a small contribution from additional waves.

[9] It is worthwhile to briefly discuss the impact of changes in wave amplitude on the longitude structure. As seen in Figure 1a, the simulation results for the *rDE*3 (dashed red) and *rSPW*4 (dashed blue) cases reveal that reducing the wave amplitude does not significantly impact the structure of the longitude variability. That is, the location of the peaks and troughs are unchanged. However, the magnitude of the longitude variability is reduced. In both cases the 50% reduction in wave amplitude results in a ∼50% reduction in peak-to-trough amplitude of the vertical **E** × **B** drift velocity. Changes in the *DE*3 or *SPW*4 can thus be considered to drive similar magnitude (in a relative sense) changes in the wave-4 structure.

[10] We now turn our attention to the impact of the *DE*3 and *SPW*4 on low-latitude F-region electron densities. We neglect the *SE*2 since, as previously demonstrated, it does not contribute to the wave-4 longitude variation in vertical **E** × **B** drift velocity. Results (not shown) further reveal that the *SE*2 does not impact the F-region ionosphere through either changes in neutral composition or winds. Figure 1b shows the longitude variation of the F-layer peak density (NmF2) at 15°N magnetic latitude averaged between 14 and 18 local time. The NmF2 values are presented for 15° magnetic latitude since this corresponds to the northern equatorial ionization anomaly crest. The NmF2 values are

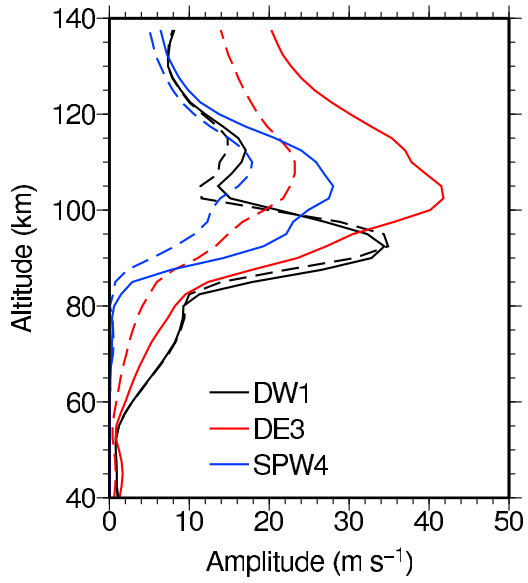

Figure 2. Equatorial profiles of the amplitude of *DW*1, *DE*3, and *SPW*4 in zonal wind based on the TIME-GCM simulations. Solid lines correspond to model results with GSWM-02 migrating and nonmigrating tides applied at the model lower boundary. Dashed lines are for the simulation results where the amplitude of the *DE*3 tidal forcing was reduced by 50% at the model lower boundary.

averaged over a later local time than the vertical **E** × **B** drifts since the wave-4 variation in NmF2 is most prominent a few hours after the wave-4 variation in **E** × **B** drifts [e.g., *Fang et al.*, 2009]. Figure 1b also includes the observed NmF2 variation based on observations from the Constellation Observing System for Meteorology Ionosphere and Climate (COSMIC) satellites. The COSMIC data were obtained through the COSMIC Data Analysis and Archive Center (CDAAC, http://cdaac-www.cosmic.ucar.edu/cdaac/) and are averaged over ±30 days from September equinox during 2008. Comparison of the model results for the realistic case and the COSMIC observations reveals some similarities and differences. Both the realistic case (dashed black) and the COSMIC observations (dashed grey) exhibit a wave-4 variation in longitude, with enhanced NmF2 values around 90°, 180°, and 360° longitude. There is, however, a discrepancy between the location of the NmF2 enhancement near ∼270° longitude. The magnitude of the wave-4 variation is also greater in the COSMIC observations than the model simulations. These differences may be related to interannual variability in the tides which is not accounted for in the GSWM-02. Despite these differences, the similarities in the longitude structure of the realistic case and the COSMIC observations demonstrates that the model simulations generally reproduce the observed features.

[11] The impact of migrating tides, *DE*3, and *SPW*4 on producing longitude variability in NmF2 is similar to their impact on the vertical **E** × **B** drift velocity. When only migrating tides are considered, longitude variations are again apparent due to the influence of the geomagnetic field. It is again clear that the results for the *DE*3 (solid red) and *SPW*4 (solid blue) cases do not fully account for the longitude variations that are simulated in the realistic case. This further illustrates that the wave-4 variation is not due solely to the *DE*3, rather it is due to the combined effects of the *DE*3 and *SPW*4. The wave-4 longitude variation in NmF2 may be driven by vertical **E** × **B** drift variations, changes due to neutral composition, or neutral wind effects [e.g., *England et al.*, 2010]. To assess the contribution of the vertical **E** × **B** drifts, we have performed additional simulations where the vertical drifts in the ionosphere-electrodynamics model are replaced by climatological values given by *Scherliess and Fejer* [1999]. Despite the absence of a wave-4 variation in the climatological vertical **E** × **B** drift velocities (see Figure 1a, dashed grey), a wave-4 variation is still apparent in NmF2 for the *DE*3*nodyn* (dashed red) and *SPW*4*nodyn* (dashed blue) simulation results. Neutral composition and winds therefore also contribute to the production of the daytime wave-4 longitude variation. Additional simulations (not shown) using climatological **E** × **B** drift velocities and only using the *DE*3, or *SPW*4, to reconstruct the neutral winds (i.e., the neutral composition and temperature are reconstructed using only migrating tides) reveal that the longitude variability in the NmF2 is due primarily to meridional neutral wind effects. Interestingly, the location of the maxima and minima in longitude differs between the *DE*3 and *DE*3*nodyn* cases as well as between the *SPW*4 and *SPW*4*nodyn* cases. This indicates that at certain longitudes the effects of the neutral composition and winds will compliment the vertical **E** × **B** drifts, while at other longitudes the two are in opposition. For understanding the complete longitude variability, it is therefore important to consider the combined effects of neutral composition, winds, and vertical **E** × **B** drifts.

[12] The results presented clearly illustrate that both the *DE*3 and *SPW*4 influence the generation of wave-4 longitude variability in the low-latitude ionosphere. We now briefly discuss the connection between these two waves. The *SPW*4 is not forced at the TIME-GCM lower boundary, and it is thus generated through processes internal to the model. As discussed by *Hagan et al.* [2009], the most likely scenario is that the *SPW*4 is generated by nonlinear interaction between the *DE*3 and *DW*1. If this is the case, changes in the *DE*3 (or the *DW*1) should also result in changes in the *SPW*4. Figure 2 shows equatorial profiles of the *DW*1, *DE*3, and *SPW*4 in zonal neutral wind for TIME-GCM simulations using the GSWM forcing, and for the TIME-GCM simulations where the *DE*3 forcing from the GSWM at the lower boundary was reduced by 50%. The equatorial profiles in Figure 2 can be considered as representative of the tidal behavior throughout the low-latitude region. The 50% reduction in the *DE*3 forcing at the model lower boundary results in a ∼50% reduction in the peak *DE*3 amplitude. Although a 50% change in *DE*3 may appear extreme, we note that simulation results reveal the occurrence of day-to-day variability of this magnitude (H.-L. Liu, WACCM-X Simulation of Upper Atmosphere Wave Variability, submitted to *Geophysical Monograph Series*, 2012). The maximum *SPW*4 amplitude is also reduced, however, the reduction is only ∼10 ms^{-1}, or about 30%. The reduction in the *SPW*4 that occurs when the *DE*3 is reduced supports the hypothesis of *Hagan et al.* [2009] that the *SPW*4 is generated through the nonlinear interaction of the *DE*3 and *DW*1. This further elucidates the interconnection between these two waves and demonstrates that variability in the *DE*3, or perhaps the *DW*1, can drive a similar variation in the *SPW*4. This connection is important to consider, especially since as

we have shown both the *DE*3 and *SPW*4 are important for generating longitude variations in the ionosphere.

4. Conclusions

[13] In the present study we have investigated the origin of the wave-4 longitude variation in the low-latitude ionosphere during September equinox. Our results clearly indicate that, although the *DE*3 alone produces a wave-4 longitude variation, it is not the sole contributor to the wave-4 longitude variation. We find that the *SPW*4 also contributes to the wave-4 longitude variation in the daytime vertical $\mathbf{E} \times \mathbf{B}$ drift velocities as well as the NmF2. As demonstrated by our TIME-GCM simulations, the *SPW*4 is generated by the nonlinear interaction of the *DE*3 and *DW*1, and *SPW*4 variability can be driven by changes in the *DE*3. While the *DE*3 and *SPW*4 are both found to generate wave-4 longitude variability in the low-latitude ionosphere, the *SE*2 does not appear to have any significant influence on ionospheric longitude variability. Our results further demonstrate that the wave-4 longitude variability that occurs near September equinox is primarily driven by the combined effects of the *DE*3 and *SPW*4. Therefore, in addition to the *DE*3, it is vital that future studies also consider the *SPW*4 as a contributor to the wave-4 longitude variation in the low-latitude ionosphere during September equinox. This is of particular importance when considering the source of variability in the wave-4 longitude structure, and we emphasize that both the *DE*3 and *SPW*4 should be considered as potential sources of this variability.

[14] **Acknowledgments.** The National Center for Atmospheric Research is sponsored by the National Science Foundation. This work was supported in part by a NCAR Advanced Study Program Postdoctoral Fellowship (N. Pedatella). AM is supported in part by NASA grant NNX09AN57G.

[15] The Editor thanks two anonymous reviewers for assisting in the evaluation of this paper.

References

England, S. L., S. Maus, T. J. Immel, and S. B. Mende (2006), Longitudinal variation of the E region electric fields caused by atmospheric tides, *Geophys. Res. Lett.*, *33*, L21105, doi:10.1029/2006GL027465.

England, S. L., T. J. Immel, J. D. Huba, M. E. Hagan, A. Maute, and R. DeMajistre (2010), Modeling of multiple effects of atmospheric tides on the ionosphere: An examination of possible coupling mechanisms responsible for the longitudinal structure of the equatorial ionosphere, *J. Geophys. Res.*, *115*, A05308, doi:10.1029/2009JA014894.

Fang, T.-W., H. Kil, G. Millward, A. D. Richmond, J.-Y. Liu, and S.-J. Oh (2009), Causal link of the wave-4 structures in plasma density and vertical plasma drift in the low-latitude ionosphere, *J. Geophys. Res.*, *114*, A10315, doi:10.1029/2009JA014460.

Fejer, B. G., J. W. Jensen, and S.-Y. Su (2008), Quiet time equatorial F region vertical plasma drift model derived from ROCSAT-1 observations, *J. Geophys. Res.*, *113*, A05304, doi:10.1029/2007JA012801.

Forbes, J. M., X. Zhang, S. Palo, J. Russell, C. J. Mertens, and M. Mlynczak (2008), Tidal variability in the ionospheric dynamo region, *J. Geophys. Res.*, *113*, A02310, doi:10.1029/2007JA012737.

Hagan, M. E., and J. M. Forbes (2002), Migrating and nonmigrating diurnal tides in the middle and upper atmosphere excited by tropospheric latent heat release, *J. Geophys. Res.*, *107*(D24), 4754, doi:10.1029/2001JD001236.

Hagan, M. E., and J. M. Forbes (2003), Migrating and nonmigrating semidiurnal tides in the upper atmosphere excited by tropospheric latent heat release, *J. Geophys. Res.*, *108*(A2), 1062, doi:10.1029/2002JA009466.

Hagan, M. E., A. Maute, R. G. Roble, A. D. Richmond, T. J. Immel, and S. L. England (2007), Connections between deep tropical clouds and the Earth's ionosphere, *Geophys. Res. Lett.*, *34*, L20109, doi:10.1029/2007GL030142.

Hagan, M. E., A. Maute, and R. G. Roble (2009), Tropospheric tidal effects on the middle and upper atmosphere, *J. Geophys. Res.*, *114*, A01302, doi:10.1029/2008JA013637.

Immel, T. J., E. Sagawa, S. L. England, S. B. Henderson, M. E. Hagan, S. B. Mende, H. U. Frey, C. M. Swenson, and L. J. Paxton (2006), Control of equatorial ionospheric morphology by atmospheric tides, *Geophys. Res. Lett.*, *33*, L15108, doi:10.1029/2006GL026161.

Lin, C. H., C. C. Hsiao, J. Y. Liu, and C. H. Liu (2007), Longitudinal structure of the equatorial ionosphere: Time evolution of the four-peaked EIA structure, *J. Geophys. Res.*, *112*, A12305, doi:10.1029/2007JA012455.

Millward, G. H., A. D. Richmond, T. J. Fuller-Rowell, and A. D. Aylward (2007), Modeling the effects of changes in the terrestrial magnetic field on the climatology of the mid- and low-latitude ionosphere *Eos Trans. AGU*, *88*(52), Fall Meet. Suppl., Abstract SA21B-08.

Oberheide, J., J. M. Forbes, X. Zhang, and S. L. Bruinsma (2011), Wave-driven variability in the ionosphere-thermosphere-mesosphere system from TIMED observations: What contributes to the "wave 4"?, *J. Geophys. Res.*, *116*, A01306, doi:10.1029/2010JA015911.

Roble, R. G. (1995), Energetics of the mesosphere and thermosphere, in *The Upper Mesosphere and Lower Thermosphere: A Review of Experiment and Theory*, *Geophys. Monogr. Ser.*, vol. 87, edited by R. M. Johnson and T. L. Killeen, pp. 1–21, AGU, Washington, D. C.

Roble, R. G., and E. C. Ridley (1994), A thermosphere-ionosphere-mesosphere- electrodynamics general circulation model (TIME-GCM): Equinox solar cycle minimum simulations (30–500 km), *Geophys. Res. Lett.*, *21*, 417–420, doi:10.1029/93GL03391.

Scherliess, L., and B. G. Fejer (1999), Radar and satellite global equatorial F region vertical drift model, *J. Geophys. Res.*, *104*(A4), 6829–6842, doi:10.1029/1999JA900025.

Scherliess, L., D. C. Thompson, and R. W. Schunk (2008), Longitudinal variability of low-latitude total electron content: Tidal influences, *J. Geophys. Res.*, *113*, A01311, doi:10.1029/2007JA012480.

Teitelbaum, H., and F. Vial (1991), On tidal variability induced by nonlinear interaction with planetary waves, *J. Geophys. Res.*, *96*(A8), 14,169–14,178, doi:10.1029/91JA01019.

Zhang, X., J. M. Forbes, and M. E. Hagan (2010), Longitudinal variation of tides in the MLT region: 2. Relative effects of solar radiative and latent heating, *J. Geophys. Res.*, *115*, A06317, doi:10.1029/2009JA014898.